A Two-Dimensional Volatility Basis Set: 3. Prognostic Modeling and NO$_x$ Dependence

Wayne K. Chuang[1] **and Neil M. Donahue**[1]

[1]Carnegie Mellon University Center for Atmospheric Particle Studies, Pittsburgh, USA

Correspondence to: Neil M. Donahue
(nmd@andrew.cmu.edu)

Abstract. When NO$_x$ is introduced to organic emissions, aerosol production is sometimes, but not always, reduced. Under certain conditions, these interactions will instead increase aerosol concentrations. We expanded the two-dimensional volatility basis set (2D-VBS) to include the effects of NO$_x$ on aerosol formation. This includes the formation of organonitrates, where the addition of a nitrate group contributes to a decrease of 2.5 orders of magnitude in volatility. With this refinement, we model outputs from experimental results, such as the atomic N:C ratio, organonitrate mass, and nitrate fragments in AMS measurements. We also discuss the mathematical methods underlying the implementation of the 2D-VBS and provide the complete code in the supplemental material. A developer version is available on Bitbucket, an online community repository.

1 Introduction

Aerosols, or particulate matter (PM), cause numerous cardiovascular and respiratory diseases, and chronic exposure to high concentrations can significantly reduce life expectancy (Dockery et al., 1993; Peng et al., 2005; Pope et al., 2009). Particles smaller than 2.5 micrometers (PM$_{2.5}$) directly contribute to respiratory- and cardiovascular-related deaths. This is most concerning in major cities where air pollution can reach extremely hazardous levels. In addition, PM affects ecosystems and the atmosphere, exerting significant direct and indirect forces on climate. Direct forcing comes from the scattering or absorption of solar radiation by aerosols. Indirect forcing comes from the scattering of solar radiation by clouds, which is in turn controlled by hydrophilic particles known as Cloud Condensation Nuclei (CCN) (Seinfeld and Pandis, 2006). In order to track the production of aerosols, models predict the interactions between emissions from various sources and their effects on the formation of PM.

PM$_{2.5}$ consists of a rich mixture including both inorganic and organic compounds, commonly found within individual particles. Inorganics include sodium chloride (from sea spray), sulfate (mostly from coal combustion), nitrate (mostly from high-temperature combustion), ammonium (from animal husbandry), elemental carbon (from combustion of organic fuels), and trace metals such as nickel, manganese, etc. Organics comprise 20-50% of PM$_{2.5}$ mass in the continental mid-latitudes and as much as 90% in tropical forests (Andreae and Crutzen, 1997; Kanakidou et al., 2005). The organics are called organic aerosol (OA), and while the inorganics consist of a relatively small set of compounds, OA consists of a rich mixture containing many thousands of different individual organic compounds (Goldstein and Galbally, 2007; Kroll et al., 2011).

OA comes from biogenic (naturally-occurring) and anthropogenic (human-related) sources. Biomass burning (BBOA) is the largest contributor to OA worldwide (Bond et al., 2004). Some BBOA comes from natural carbon (woodsmoke), but the combustion is largely associated with human activity and so BBOA is classified as anthropogenic. Overall, OA comprises roughly 10% of the total flux of organic carbon into (or out of) the atmosphere (Goldstein and Galbally, 2007; Hallquist et al., 2009); thus only a fraction of organic compounds have the right properties to reside in the condensed phase. The requisite property is a low volatility (Pankow, 1994; Donahue et al., 2011, 2014); to stay in the organic phase under typical conditions, an organic molecule must have a vapor pressure lower than roughly 10^{-10} atm (10^{-5} Pa, C$^* < 1\,\mu$g m^{-3}) (Donahue et al., 2011).

OA is also classified as primary or secondary (Murphy et al., 2014; Cronn et al., 1977; Turpin and Huntzicker, 1995). Primary organic aerosols (POA) are directly emitted

into the atmosphere on particles, and are largely from anthropogenic sources such as automobile exhaust and biomass burning. Secondary organic aerosols (SOA) are formed when chemical reactions cause condensation of organic compounds from the gas phase. Oxidants include ozone, hydroxyl (OH·) radicals, and nitrate (NO_3) radicals (Turpin et al., 2000), and oxidation can occur in the gas phase (Pandis et al., 1991) or in the aqueous phase (Turpin et al., 2000). Oxidation can add functional groups to an organic backbone (functionalization), forming products with a lowered volatility; however, oxidation can also lead to C-C bond cleavage (fragmentation), often forming products with an elevated volatility (Kroll et al., 2011; Chacon-Madrid et al., 2010). In addition, association reactions between relatively volatile reaction products can lead to higher molecular weight, lower vapor pressure products (oligomers) (Kalberer et al., 2004).

Oxidation of an organic compound, even one generation, generally forms many products, each with a different volatility (Atkinson et al., 1997; Aumont et al., 2005; Lim and Ziemann, 2009). Thus SOA production has been described in terms of a volatility distribution of reaction products (Odum et al., 1996; Presto and Donahue, 2006; Donahue, 2012). However, this also means that the oxidation products (and thus volatility distribution and overall SOA mass yields) often depend strongly on ambient conditions. The dominant oxidant can have a large effect (OH vs ozone during the day, NO_3 vs ozone at night), but so can the organic radical chemistry following the initial oxidation step.

One notable source of variability in SOA mass yields is the NO_x level (Presto and Donahue, 2006; Zhang et al., 2006; Ng et al., 2007; Logan et al., 1981; Thompson and Cicerone, 1982). NO_x (NO and NO_2) can react with organic radicals to change the product distribution from oxidation reactions (Atkinson et al., 1997). NO_x is most commonly formed under high-temperature conditions such as combustion; NO_x concentrations range from 10-1000 ppb in urban areas to 10 ppt in remote regions (Seinfeld and Pandis, 2006), and so NO_x is one of the most highly variable reactive trace species in the atmosphere and also one of the most potent indications of human activity. Because NO_x can alter the oxidation chemistry of organic compounds, even biogenic organic precursors (e.g. isoprene and terpenes) may in fact form "anthropogenically enhanced" SOA if the SOA mass yields are in some way enhanced by the presence of NO_x.

There is evidence that a large source of SOA associated with CO emissions (and thus presumably anthropogenic activity) is required to explain global surface OA observations (de Gouw and Jimenez, 2009; Spracklen et al., 2011). At the same time, a large fraction of OA appears to consist of modern carbon (containing ^{14}C) (Weber et al., 2007; Aiken et al., 2010; Minguillón et al., 2011; Zhang et al., 2012). This has led to speculation that interactions between biogenic precursors and urban plumes – possibly NO_x – may be responsible for the anthropogenic enhancement (Shilling et al., 2013). If so, the dramatic decline in NO_x levels in the southeast United States over the past decade (Russell et al., 2012) might be associated with a corresponding decrease in anthropogenically enhanced SOA.

Tracking any NO_x effect is thus extremely important. If changed product distributions (and thus SOA mass yields) were the sole effect of increased NO_x, then the NO_x influence could be dealt with easily by adjusting SOA mass yields based on NO_x levels (Presto and Donahue, 2006; Lane et al., 2008a). However, if there is a reason to track specific products, or if the subsequent, later-generation chemistry of the reaction products also differs substantially under high- and low-NO_x conditions, then simply adjusting mass yields will not suffice. In the case of NO_x, both of these conditions apply: there is strong evidence that the aging chemistry of SOA depends on its composition (Zhang et al., 2006; Henry and Donahue, 2012), and also that organonitrates produced under high-NO_x conditions are independently measured as a diagnostic of ambient aging conditions.

High organonitrate concentrations are typically found in areas with high NO_x levels. (Garnes and Allen, 2002; Mylonas et al., 1991) The addition of a nitrate functional group to a carbon backbone reduces volatility by $\sim$2.5 orders of magnitude (Pankow and Asher, 2008), potentially contributing to SOA formation as a result. Organonitrates can be identified on filter samples by characteristic absorption features using FTIR (Russell et al., 2011) and also in bulk mass spectra from the Aerosol Mass Spectrometer (AMS, Aerodyne Inc.) (Zhang et al., 2006; Farmer et al., 2010). Detection in the AMS is challenging because organonitrates fragment almost completely to give NO^+ (*m/z = 30*) and NO_2^+ (*m/z = 46*). The same fragments arise from (often much more abundant) inorganic nitrate; however, the fragment signal ratio (30:46) can be indicative of organonitrates and is quite distinct from ammonium nitrate (Farmer et al., 2010).

Depending on the carbon chain length, organonitrates can have a gas-phase atmospheric lifetime ranging from days to months, and thus drive long-range NO_x transport into remote marine regions (Atherton, 1989). Higher carbon number organonitrates will partition to the condensed phase (Ziemann and Atkinson, 2012). Organonitrates have been found in aerosol samples at numerous sites across North America (Russell et al., 2011). In particular, high concentrations of organonitrates have been observed in California and Texas (Garnes and Allen, 2002; Day et al., 2010). AMS data from photooxidation of α-pinene, limonene, and longifolene under high-NO_x conditions show mass fragments corresponding to the formation of organonitrates (Zhang et al., 2006; Ng et al., 2007). In some field observations, roughly 10-20% of the organic aerosol mass is comprised of organonitrates; however, organonitrates are not always found in urban areas even in high-NO_x conditions. Field data from Pittsburgh and the U.S. East Coast revealed low concentrations of aerosol organonitrates (Wittig et al., 2004; Russell et al., 2011). This may be due to the hydrolysis of organonitrates, where water reacts in the condensed phase with the nitrate group to

form an alcohol and nitric acid (inorganic nitrate) (Liu et al., 2012). The change in the functional group likely has little effect on the volatility of the compound; the -OH functional group replacing the -ONO_2 group has about the same effect on volatility (Pankow and Asher, 2008).

During daytime, organonitrates are formed through reactions of NO with organic peroxy radicals ($RO_2\cdot$). As NO_x concentrations rise, progressively more $RO_2\cdot$ react with NO instead of $RO_2\cdot$ or $HO_2\cdot$. The reaction with NO produces an intermediate product, ROONO, that can either decompose into an alkoxy radical (RO· and NO_2) or isomerize to form an organonitrate ($RONO_2$) (Atkinson et al., 1997; Zhang et al., 2004). The alkoxy radicals will further react, either forming stable organics that are more functionalized or fragmenting to produce lower carbon-number products. Organonitrate yields from ROONO rise with carbon number and decreasing temperature and vary somewhat with structure, reaching an asymptotic limit of roughly 0.3 at 300K for most compounds relevant to SOA formation (Atkinson and Arey, 2003; Ziemann and Atkinson, 2012). Alkyl nitrates for species with >20 carbons are predominantly in the particle phase (Lim and Ziemann, 2009). High-NO_x products differ from low-NO_x products; this can lead to comparatively higher or lower SOA concentrations (Presto et al., 2005; Kroll et al., 2006; Ng et al., 2007).

During nighttime, organonitrates are formed through reactions of NO_3 with unsaturated organic precursors. (Crowley et al., 2011; Rollins et al., 2009) This reaction can produce organonitrates on the same magnitude as daytime organonitrate formation. (Fry et al., 2013) However, the concentration profile of NO_3 is not well understood, and can vary widely depending on boundary layer conditions. (He et al., 2014; Fry et al., 2013) Daytime NO_3 rapidly undergoes photolysis or reacts with NO to form NO_2, and are thus typically unable to form organonitrates in the presence of light. Product distributions for NO_3 + VOC reactions have not been developed for the 2D-VBS, but its contribution to organonitrate production can eventually be incorporated within the current framework.

2 Background

2.1 Volatility Basis Set

The complexity of OA partitioning and the vast number of reaction products motivated the Volatility Basis Set (VBS). The original (one-dimensional) VBS was designed to represent partitioning and aging by lumping organic molecules only by volatility, in bins separated by an order of magnitude (at 300K) in a logarithmic volatility space (Donahue et al., 2006). In principle the 1D-VBS can be implemented with as few as 4 transportable species (a single 4-bin VBS with C^* = [1, 10, 100, 1000] $\mu g\ m^{-3}$) at the cost of losing all information about the source of the SOA. SOA models that retain information (e.g. biogenic vs anthropogenic SOA) have correspondingly more transportable species; Lane et al. (2008a) retained 4 VBS bins for each SOA precursor source. Other 1D-VBS implementations have used a wider volatility range, for example transporting 7 species with $0.01 \leq C^* \leq 10,000$ for SOA formed via oxidation of evaporated primary emissions (Shrivastava et al., 2008).

Aging schemes within the 1D-VBS employ a single coupling matrix (Donahue et al., 2006) that can vary with ambient conditions to represent changes in chemistry (Lane et al., 2008a). However, individual VBS bins can include such different species as $C_{23}H_{48}$ (tricosane) and $C_6H_{10}O_5$ (levoglucosan). There is good reason to believe that the chemistry of these species is quite different – most notably, fragmentation is likely to become more important with increasing oxygenation (Kroll et al., 2009, 2011). Furthermore, the degree of oxidation is an important diagnostic of ambient (Zhang et al., 2007; Jimenez et al., 2009) and chamber (Shilling et al., 2009; Chen et al., 2011) OA measurements. While fragmentation is described in the original 1D-VBS implementation (Donahue et al., 2006), the oxygen content is not tracked, cannot be used as a diagnostic, and cannot inform the aging chemistry.

The 2D-VBS adds a second dimension of oxygenation (O:C) or average carbon oxidation state ($\overline{OS}_C$ = 2O:C - H:C) (Donahue et al., 2011; Donahue, 2012). It was developed to capture these important defining properties of OA and track and predict changes over time.

The volatility and $\overline{OS}_C$ of organic material are represented explicitly and evolve with aging chemistry, enabling explicit description of the production and evolution of SOA over time. In addition, rate constants for reactions with OH radicals are assigned based on typical chemical structures throughout the two-dimensional space (Donahue et al., 2013). While adding complexity, this expanded representation enables much more systematic exploration of different aging mechanisms in both box-models (Donahue, 2012) and Lagrangian chemical transport models (Murphy et al., 2012). It does not, however, enable explicit tracking of product categories such as organonitrates.

Here we describe a refinement to the 2D-VBS by introducing layers to hold key product classes – organonitrates in this case. This allows us to more accurately account for the effect of NO_x on the production and evolution of SOA and to capture a more complete picture of organic aging by incorporating the production and removal of organonitrates. The model replicates experimental data on the effect of NO_x, where high-NO_x conditions increase SOA formation for certain precursors (longifolene) and decrease in others (α-pinene) (Presto et al., 2005; Pathak et al., 2007; Kroll et al., 2006; Ng et al., 2007).

Mathematically, all implementations of the VBS are formally one-dimensional: an array of species is connected via a chemical coupling matrix that describes transformations due to aging reactions. However, the physical properties repre-

sented by that array of species can be cast into multiple dimensions – volatility, oxidation state, and now levels of key molecular classes. As part of the online supplemental material for this paper we have released a full implementation of the VBS, coded in MATLAB, providing full graphical diagnostics, access to the different levels of complexity (1D, 2D, layered), and instructions for alteration and expansion (e.g. changing volatility or oxidation state ranges, adding layers, etc.). In addition, more recent and updated versions of the code are stored in the online repository Bitbucket; instructions are detailed within the supplemental material.

2.2 Mathematical overview

The 2D-VBS follows the movement of carbon mass throughout the volatility and $\overline{\mathrm{OS}}_C$ space by modeling the basic aging processes of functionalization and fragmentation. Functionalization adds functional groups, producing more oxidized organics that have lower volatility than the parent compound. Fragmentation splits the carbon backbone of an oxidized compound, producing two smaller compounds of higher volatility and generally higher $\overline{\mathrm{OS}}_C$ (Donahue, 2012). The 2D-VBS implements these aging processes as a series of matrix manipulations.

While the 2D-VBS is typically presented as a two-dimensional space, it is implemented as a one dimensional concentration vector in the code.

The mass of carbon ($C_{v,o}$) in $\mu\mathrm{g}\,\mathrm{m}^{-3}$ is described in each cell (v,o), where v is the volatility (x) index and o is the oxidation (y) index. This can be transformed into a single row vector C with n elements, or cells, $n = v \times o$. The transformation method concatenates the rows (the volatilities of each O:C) together:

$$\begin{bmatrix} C_{1,1} & \cdots & C_{x,1} \\ \vdots & \ddots & \vdots \\ C_{1,y} & \cdots & C_{x,y} \end{bmatrix} \rightarrow \begin{bmatrix} C_{1,1} \cdots C_{x,1} \; C_{1,2} \cdots C_{x,2} \cdots C_{1,y} \cdots C_{x,y} \end{bmatrix}$$
$$(1)$$

The addition of dimensions, such as organonitrates, is implemented the same way by extending the one dimensional array to track these compounds.

Chemical reactions can then be represented as transformations from an initial cell i to all potential final cells f; each transformation T is a column vector of length n, with $\sum_f T_f = 1$ (the transformations conserve carbon). The n transformation vectors for each initial cell i can then be concatenated to form an $n \times n$ transformation matrix, $\mathbf{T} = [\boldsymbol{T}_1...\boldsymbol{T}_n]$. The overall chemical transformation is then given by $C\mathbf{T}$.

The rate at which components react with OH (or any other oxidant) depends on their composition. Molecules with more carbons typically have more hydrogens available for abstraction reactions. Additionally, the more oxygens a molecule has, the more it is destabilized, and the more likely it will react. (Kwok and Atkinson, 1995) However, when enough functional groups become attached to the carbon backbone, the remaining hydrogen atoms are typically less reactive, and so reactivity decreases. A composition-activity relationship from (Donahue et al., 2013) accounts for these factors and is used to approximate rate constants gas-phase reactivity for each cell in the VBS. These values form a gas-phase reactivity vector, $\boldsymbol{k}^{\mathrm{vap}}$:

$$\boldsymbol{k}^{\mathrm{vap}} \simeq 1.2\times10^{-12}(n_C + 9n_O - 10(\mathrm{O}\!:\!\mathrm{C})^2)\,\mathrm{cm}^3\,\mathrm{molec}^{-1}\,\mathrm{s}^{-1}$$
$$(2)$$

where n_C and n_O correspond to the number of carbon and oxygen atoms, respectively.

We also parametrize the chemistry following the initial reaction with OH. The probabilities of fragmentation and functionalization are represented by vectors $\boldsymbol{f}^{\mathrm{frag}}$ and $\boldsymbol{f}^{\mathrm{func}}$, respectively, where $\boldsymbol{f}^{\mathrm{frag}} = (\mathrm{O}\!:\!\mathrm{C})^{\mathrm{n}}$ and $\boldsymbol{f}^{\mathrm{func}} = 1 - \boldsymbol{f}^{\mathrm{frag}}$. The formula for the potential for fragmentation is determined by the higher likelihood of fragmentation when a molecule is highly oxidized, because of the destabilizing effect of functional groups on the carbon backbone. The exponent, n, expresses the strength of fragmentation reactions, and is currently estimated to be $\frac{1}{4}$ (Donahue et al., 2012).

Functionalization kernels are created using a distribution based on the degree of oxidation of the compound. The kernel is defined in terms of a probability distribution for added oxygen and decreased volatility. (Donahue et al., 2012) That distribution is then mapped onto the C^o, O:C space to form a functionalization transformation array. For each volatility cell i, functionalization ($\boldsymbol{T}_i^{\mathrm{func}}$) distributes carbon mass throughout the n VBS cells.

Fragmentation kernels describe the distribution of organic material throughout (mostly) higher volatility bins and O:C following cleavage of the carbon backbone. Some fragmentation products are molecules and some are radicals, which in turn are rapidly functionalized; the fragmentation kernel describes the ultimate distribution of stable products from this process and thus distributes carbon over a much wider range of the VBS than functionalization. (Donahue et al., 2012) The overall transformation vector $\boldsymbol{T}_i$ is found for functionalization and fragmentation by combining the two processes together, $\boldsymbol{T}_i = \boldsymbol{f}_i^{\mathrm{frag}} \cdot \boldsymbol{T}_i^{\mathrm{frag}} + \boldsymbol{f}_i^{\mathrm{func}} \cdot \boldsymbol{T}_i^{\mathrm{func}}$. Also, $\sum_{f=1}^{n} T_{i,f} = 1$, meaning carbon mass is conserved. Concatenated over all columns, $i = 1...n$, the transformations form the transformation matrix $\mathbf{T}$. The aging process is then expressed as:

$$\frac{\partial C}{\partial t} = \boldsymbol{k^{vap}} \cdot [OH] \cdot \boldsymbol{C}\,(\mathbf{T} - \mathbf{I})$$
$$(3)$$

This can be modeled with differential solvers in MATLAB.

The transformations just described apply to species in the vapor phase. The VBS separately tracks vapor (C^{vap}) and condensed (C^{cond}) phase concentrations. For the condensed phase, the OH rate constant is specified as an effective gas-phase rate constant, k_i^{eff}, which is determined by the

diffusion-limited uptake of gas-phase OH by particles, based on the Fuchs corrected surface area of a given particle size distribution (Donahue et al., 2013). We generally assume this is independent of composition and that OH reacts with unit efficiency once it reaches the surface of a particle. Lacking other constraints, we assume that $\boldsymbol{f}^{\text{func}}$ and $\boldsymbol{f}^{\text{frag}}$ are the same in the gas and condensed phases, so $\boldsymbol{T}^{\text{vap}} = \boldsymbol{T}^{\text{cond}}$; however, it is likely that even the functionalization and fragmentation kernels differ in the gas and condensed phases, so we anticipate that future refinements will remove this assumption.

Additional details on the distribution of material throughout the VBS may be found in Donahue et al. (2012) and Murphy et al. (2012).

2.3 Treatment of Organonitrates

The introduction of NO_x to the system brings additional chemical reactions and the potential to form organonitrates through the functionalization process. Organonitrates are accounted for in a separate layer of the 2D-VBS, called the "N_1" layer for the inclusion of an atomic nitrogen. The addition of a nitrate group decreases the volatility by ~ 2.5 orders of magnitude (Pankow and Asher, 2008) and increases the number of oxygens attached to the carbon backbone by 1 (the other oxygen atoms and the nitrogen constitute an NO_2 group).

This has the potential to produce high concentrations of organonitrates in the condensed phase because of the large decrease in the volatility of the product compared to the reactant.

The formation of an organonitrate involves two branch points. The first is the probability $(1-\beta)$ that RO_2 will react with NO; the second is the yield, η, of organonitrates from $RO_2 + NO$. The nitrate yield η rises with increasing carbon number (Arey et al., 2001; Yeh and Ziemann, 2014) and depends on the functionality of the RO_2 (Lim and Ziemann, 2009; Elrod, 2011); however, for organics large enough to partition to the condensed phase, η is at an asymptotic limit, and we assume a homogeneous distribution of RO_2 structures within any given VBS cell. We thus assume that $\eta = 0.30$ in all cases. Various ways of estimating β are possible, such as from the VOC:NO_x ratios obtainable in experimental data, (Presto et al., 2005) to the comparison of the rates of reaction between $RO_2 + NO$ and $RO_2 + HO_2$. (Lane et al., 2008b) In this work, we will simply vary β parametrically.

There are now three different transformation pathways for organics in the N_0 (non-organonitrate) layer: they can fragment, functionalize without forming organonitrates, or form organonitrates. As a simplification, we assume that there are two pathways for organonitrates in the N_1 layer: they can fragment by eliminating the NO_2 group and return to the N_0 layer, or they can functionalize and remain in the N_1 layer. Also as a simplification we assume that dinitrates with $2 - ONO_2$ functional groups are minor products, and so we

do not add an N_2 layer. The transformations for the organonitrate case are analogous to the non-organonitrate case, but with expansions to accommodate the production and loss of organonitrates. The concentration array doubles in size: $\boldsymbol{C} = \begin{bmatrix} \boldsymbol{C}_{N_0} \boldsymbol{C}_{N_1} \end{bmatrix}$, where $\boldsymbol{C}_{N_0}$ represents all the cells in the N_0 layer and $\boldsymbol{C}_{N_1}$ represents the cells in the N_1 layer. More complex is the transformation matrix, which is now:

$$\mathbf{T} = \begin{bmatrix} \mathbf{T}_{N_0 \to N_0} & \mathbf{T}_{N_0 \to N_1} \\ \mathbf{T}_{N_1 \to N_0} & \mathbf{T}_{N_1 \to N_1} \end{bmatrix} \tag{4}$$

where: $\mathbf{T}_{N_0 \to N_0}$ represents the original functionalization and fragmentation of the non-organonitrate layer. $\mathbf{T}_{N_0 \to N_1}$ is the formation of an organonitrate through functionalization. $\mathbf{T}_{N_1 \to N_0}$ is the fragmentation of an organonitrate. $\mathbf{T}_{N_1 \to N_1}$ is the functionalization of an organonitrate. The organonitrate (N_1) layer of the 2D-VBS contains only one nitrate group, and thus each species contains a single nitrogen atom. Because n_N is constant, N:C drops as volatility decreases and the chemical species become larger. In addition, the oxygen attached to the carbon from the nitrate group contributes to the O:C of the overall compound. Therefore, the O:C of an organonitrate can never be 0. Figure 1 shows N:C for the nitrate layer (N_1) of the 2D-VBS. In the regime where aerosols tend to form under atmospheric conditions, N:C ranges from 0.04 to 0.3. Semi-volatile organonitrates have N:C from around 0.05 to 0.3; extremely low volatility compounds have an N:C lower than 0.2.

N:C for ambient aerosols are experimentally obtainable through Atomic Mass Spectroscopy (AMS). (Rollins et al., 2010) tested compounds that act as aerosol precursors in the atmosphere using the AMS, and the data from elemental analyses of these organic hydroxynitrates showed N:C ranging from 0.02 to 0.1. Other experiments of SOA production from isoprene, toluene, and naphthalene in high-NO_x conditions show N:C ranging from .04 to .08, indicating the existence of low volatility compounds with moderate levels of oxygenation. (Chhabra et al., 2010) In addition to providing a sense of the range of N:C expected in aerosols, Figure 1 also reveals the relationship between N:C and the size of the molecule itself. Molecules with very small N:C actually indicate high carbon content, meaning these organonitrates are, on a per molecule basis, contributing significant mass to the overall organic aerosol.

2.4 Time evolution

Once the transformation matrix $\mathbf{T}$ has been specified for any VBS configuration, the time evolution is trivially specified. A final detail is that we separate vapor-phase and particle-phase processes to treat the very different kinetics of homogeneous and heterogeneous oxidation. (Donahue et al., 2013) This also facilitates dynamical treatments of aerosol processes. (Trump et al., 2014; Trump and Donahue, 2014) We can also treat oligomerization within the condensed phase (Trump and Donahue, 2014), though we shall not address that here.
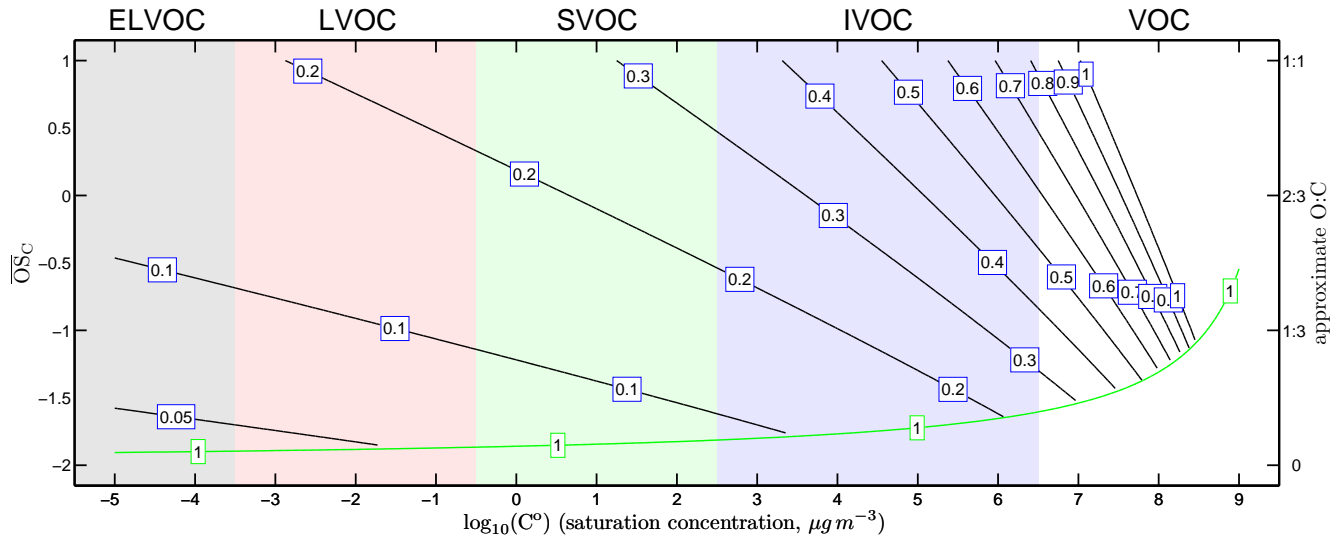
Fig. 1. Atomic N:C ratio isopleths in the organonitrate layer of the 2D-VBS. Broad volatility ranges are shown with the colored background. The volatility space is divided into regions of organic compounds: extremely low volatility (ELVOC), low volatility (LVOC), semi-volatile (SVOC), intermediate volatility (IVOC), and volatile (VOC). Most organonitrate aerosols will have an N:C ratio lower than 0.2. The green line represents the single oxygen isopleth under which no organonitrate exists, because organonitrates themselves contribute an oxygen to the O:C ratio.

Formally, this again requires that we double the concentration array to distinguish vapor- and condensed-phase concentrations: $C = \begin{bmatrix} C^{\text{vap}} & C^{\text{cond}} \end{bmatrix}$. The transformation matrix becomes:

$$\mathbf{T} = \begin{bmatrix} \mathbf{T}^{\text{vap}} & 0 \\ 0 & \mathbf{T}^{\text{cond}} \end{bmatrix} \tag{5}$$

This is block diagonal because we do not treat particle microphysics – condensation and evaporation – at this stage. That is left to a later step via operator splitting, whether we assume equilibrium partitioning or specifically treat the dynamics.

The change in the mass within each cell is described by n differential equations. For each cell i out of a total of n cells in the VBS,

$$\frac{dC}{dt} = C_{\text{OH}} \left[(\boldsymbol{k} \cdot \boldsymbol{C}) \, \mathbf{T} - (\boldsymbol{k} \cdot \boldsymbol{C}) \right] = C_{\text{OH}} \, (\boldsymbol{k} \cdot \boldsymbol{C}) \left[\mathbf{T} - \mathbf{I} \right] \tag{6}$$

where the first term is the amount of mass that is reacted into the cell from all other cells, and the second term is the loss from reactions out of the cell.

Any differential equation solver can be employed to solve Eq. 6. We currently use the approximation $exp(-k\Delta t) \approx 1 - k\Delta t$ for small Δt.

As functionalized products shift into lower volatility cells, they can condense into the aerosol phase. At equilibrium this is given by:

$$\xi_i = (1 + \frac{C_i^*}{C_{\text{OA}}})^{-1} \; ; \; C_{\text{OA}} = \sum_i C_i^* \xi_i \tag{7}$$

where C^* is the volatility (in μg m^{-3}) of the compound, ξ is the fraction of organics in the condensed phase, and C_{OA} is the total organic aerosol mass. This is a constant balancing act – if more functionalized material with lower volatility form and more mass condense, some higher volatility products will also condense. The reverse is also true – if fragmentation becomes dominant and higher volatility products form, lower volatility products may enter the vapor phase.

3 Results and Discussion

Prior VBS model implementations have treated ozonolysis and subsequent OH multi-generational aging of α-pinene in chamber studies. A 2D-VBS model reproduced aerosol mass well throughout the course of the MUCHACHAS experiments, which studied SOA aging under similar conditions in four different chambers (Donahue et al., 2012). Building upon this, the current version (v1.0 in Bitbucket) of the 2D-VBS model can also model α-pinene aging under high-NO$_x$ conditions with both ozonolysis aging and OH aging periods. While there are currently few high-NO$_x$ experimental data addressing multi-generational aging, mass yields of first-generation products from ozonolysis of α-pinene are available (Pathak et al., 2007; Presto et al., 2005). Simulations for high-NO$_x$ cases are run based on this data.

In the examples shown, we run the model under ideal chamber conditions, where there are no wall losses. A concentration of 100 μg m^{-3} of α-pinene is introduced into the chamber. For the first two hours, we model dark conditions with a constant ozone level of 300 ppbv. The ozone reacts
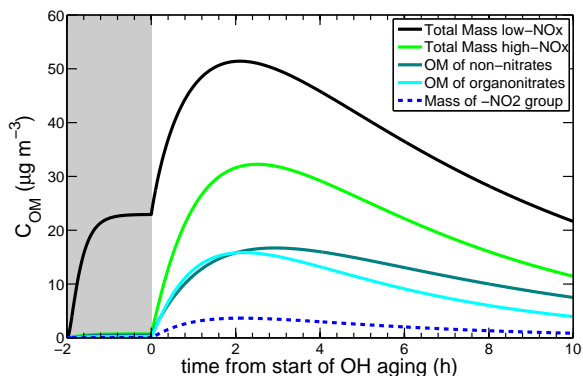
Fig. 2. Organic mass concentration over 2 hours of dark ozonolysis followed by 10 hours of OH aging for low-NO_x and high-NO_x conditions. The OM for non-nitrates and organonitrates plots are under high-NO_x conditions. High-NO_x conditions decrease the overall organic aerosol mass produced throughout the course of a model run. At $\beta = 0.15$ (85% RO_2+NO), the mass concentration of organonitrates is roughly equivalent to the mass concentration of non-organonitrates. While the contribution of the $-NO_2$ group itself is small, the organonitrate compounds can comprise a significant portion of the overall mass.

with the unsaturated carbon bonds to form first-generation products. At the end of two hours, after all of the precursor material has been reacted to form first-generation products, OH is introduced into the chamber at a constant 10^7 molecules cm^{-3} for 10 hours. This is the equivalent of turning on the UV lights in a chamber with a strong OH precursor such as HONO. The continued reaction of organic compounds creates multi-generational products, many of which are low volatility and condense into the aerosol phase. We have taken a low- and high-NO_x case, where $\beta = 1$ and $\beta = 0.15$, respectively, and examined the differences in aerosol production during first generation chemistry and subsequent multi-generation chemistry.

Figure 2 shows the differences in concentration of aerosol mass produced under low- and high-NO_x conditions throughout the course of the chamber model run. During first generation chemistry, high-NO_x conditions form very little aerosol mass, while low-NO_x conditions produce high SOA mass. This is due to higher volatility compounds that are generated because of the presence of NO_x, instead of the semi-volatile compounds in the absence of NO_x. When OH aging begins at low NO_x, the aerosol mass more than doubles as volatile compounds react to form highly functionalized, low volatility species. An even more dramatic effect is seen in the OH aging of high-NO_x first generation compounds. While most first generation products were too volatile to condense, subsequent aging pushed a significant portion of these organics into the aerosol phase. Under these model conditions, even with the dramatic increase in concentration, the high-

NO_x condition produces less overall mass during OH aging. This alternate pathway results in a significant contribution by organonitrates to the overall aerosol mass – organonitrates comprised nearly half of the total organic mass at one point during OH aging. While the mass of organonitrates is significant, if the AMS were to test this sample, it would measure only a small concentration of N-containing mass fragments (indicated with the dashed blue curve in the figure). In essence, these are very large organonitrate molecules that have significant impact on overall aerosol mass.
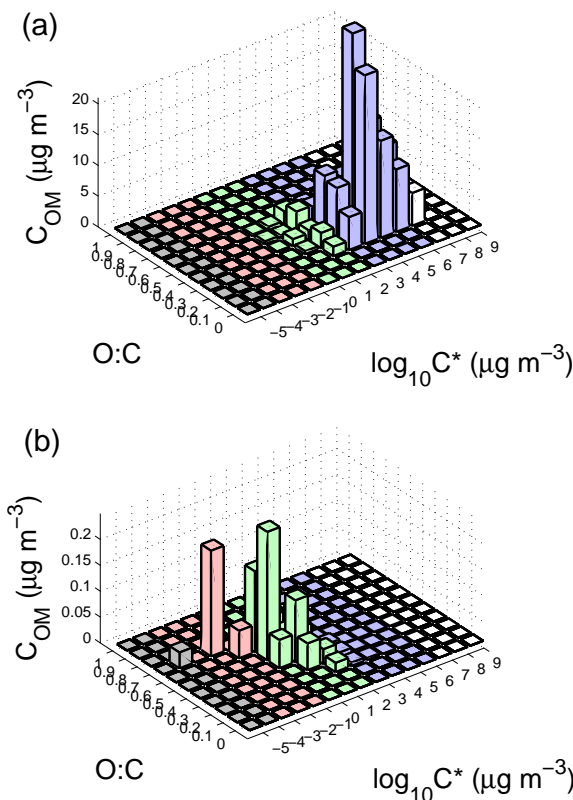

Fig. 3. Mass of first generation products for each cell in the 2D-VBS, from 100 μg m^{-3} α-pinene + ozone at $\beta = 0.15$. (a) total mass of all (organonitrate and non-nitrate) organics in both the suspended and vapor phases. (b) total mass of all organics in only the suspended phase. The suspended phase concentration axis is 2 orders of magnitude smaller than the vapor phase; most of the first generation mass remains in the vapor phase.

The distribution of mass under high-NO_x conditions offers insight into the low mass production during first generation aging. Figure 3 shows the first generation distribution (at t = 0 of Figure 2) of organics when $\beta = 0.15$. This distribution is based on chamber experiments by Pathak et al. (2007) and Presto et al. (2005) of α-pinene ozonolysis under high-NO_x concentrations. Figure 3a shows the distribution

of all organics (both aerosol and vapor phase). The majority of the organics reside in the IVOC range, which is too volatile to condense in the typical mass loadings of the atmosphere. Figure 3b shows the distribution of total suspended mate-
5 rial, comprised of both organonitrates and non-nitrates. This mass contains more oxidized material than those in the vapor phase, and range from LVOC to SVOC. Compared to the first generation distribution in low-NO_x conditions shown in Figure 2, the high-NO_x condition produces less aerosol mass
10 because of the overall higher volatilities of resulting compounds.
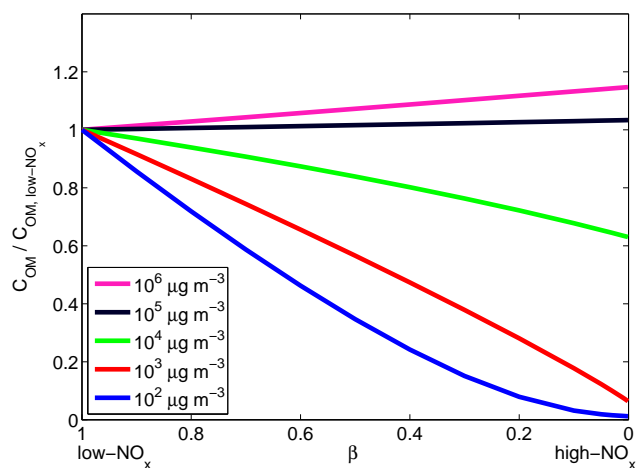

Fig. 4. The effect of peroxy-radical branching on the first-generation secondary organic aerosol concentration, C_{OM}. The x axis is the branching ratio for RO_2 reaction (β), where β=1 corresponds to low-NO_x conditions dominated by $RO_2 + HO_2$ and β=0 corresponds to high-NO_x conditions dominated by $RO_2 + NO$. The y axis is the ratio of C_{OM} at a given value of β to the low-NO_x value. Each curve represents a different amount of oxidized precursor, spanning 5 orders of magnitude from 10^2 to 10^6 $\mu g\,m^{-3}$.

The previous figures have shown that the presence of NO_x decreases aerosol mass production for α-pinene under moderate loadings. Less volatile precursors like sesquiterpenes
15 are affected differently by NO_x. A precursor with a lower volatility than α-pinene, such as longifolene, produces products with correspondingly lower volatility. (Ng et al., 2007) While first generation distributions for these precursors are currently lacking, we can emulate this effect by increasing
20 the mass loading of α-pinene instead. A precursor compound that is an order of magnitude less volatile than α-pinene can be modeled by an order of magnitude increase in mass loading. Figure 4 shows a comparison of first generation aerosol concentration under various β and mass loadings to the mass
25 concentration produced under low-NO_x. This shows that for lower mass loadings of α-pinene such as 100 $\mu g\,m^{-3}$, increasing NO_x levels decreases resultant mass. As the loadings increase in magnitude, the aerosol suppression effect of NO_x decreases. When loadings reach 10^5 $\mu g\,m^{-3}$, the effect

is reversed, instead producing more mass as NO_x levels in-
30 crease. This has been shown in experimental data from Ng et al. (2007), where longifolene exhibit higher yields under high-NO_x conditions than low-NO_x conditions. Even though the presence of NO_x produces first generation compounds from longifolene that are higher in volatility than first genera-
35 tion compounds produced under low NO_x, these compounds are still LVOCs and SVOCs, and partition into the aerosol phase. In addition, the organonitrate group contributes significant mass to the aerosol phase, resulting in the >1 high-NO_x to low-NO_x organic mass ratio. Depending on the volatility
40 of the organic precursor, it is therefore possible for the presence of NO_x to increase or decrease the total first generation aerosol mass.

As these first generation products undergo multi-generational chemistry, becoming a more complex mix of
45 organics, the stark differences between the mass loadings under first generation chemistry are dampened. Figure 5 shows the comparison between different β and different initial mass loadings with respect to the low-NO_x ($\beta = 1$) case, after 10 hours of OH aging. This corresponds to the end of the time
50 period in Figure 2. While higher loadings continue to produce more aerosol mass, an increase in NO_x now consistently produces lower mass. This comes from the tendency to cleave the nitrate group during fragmentation, decreasing the effect of the nitrate group on overall mass. In addition,
55 the probability of fragmentation increases as functionalization continues throughout the course of aging, contributing to the loss of organonitrates and the loss of aerosol mass to the vapor phase.

The distribution of suspended mass throughout the VBS
60 also changes over the course of OH aging. Figure 6 shows the distribution of mass in the 2D-VBS for the organonitrate layer (Figure 6a) and the non-nitrate (Figure 6b) after 10 hours of OH aging. This corresponds to the endpoints of the "OM of organonitrates" and "OM of non-nitrates" lines
65 in Figure 2. The organonitrate concentration is fairly small, and they are only moderately oxidized, while the non-nitrate organics are highly oxidized. Each cell of the organonitrate layer, with higher mass yet lower carbon numbers, is slower to react compared to the corresponding cell in the
70 non-nitrate layer. However, as the organonitrates undergo repeated functionalization, fragmentation of the products become more preferable, leaving behind less oxidized material in the organonitrate layer. Fragmentation of these highly functionalized organonitrates cleaves the nitrate group, re-
75 sulting in highly oxidized non-nitrate organics. As a result, the organonitrate layer tends to be less oxidized and semi-volatile while non-nitrates are highly oxidized.

4 Conclusions

We have added a layer to the 2D-VBS to account for
80 organonitrates. In addition, we have developed a module to
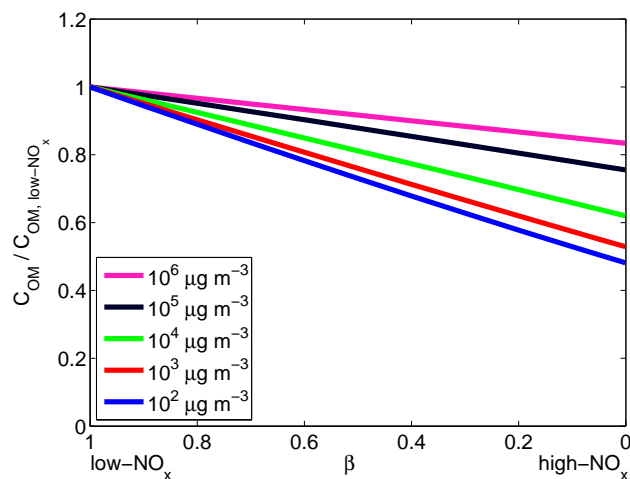
Fig. 5. The effect of peroxy-radical branching on the aged secondary organic aerosol concentration, C_{OM} after 10 hours of oxidation by 10^7 OH cm^{-3}. As in Fig. 4 the x axis is the branching ratio for RO_2 reaction (β), where $\beta=1$ corresponds to the low-NO$_x$ conditions dominated by $RO_2 + HO_2$ and $\beta=0$ corresponds to high-NO$_x$ conditions dominated by $RO_2 + NO$. The y axis is the ratio of C_{OM} at a given value of β to the low-NO$_x$ value. Each curve represents a different amount of oxidized precursor, spanning 5 orders of magnitude from 10^2 to 10^6 μg m^{-3}.

Fig. 6. The distribution of mass is plotted over the 2D-VBS space for multi-generation products, after 10 hours of OH aging of 100 μg m^{-3} α-pinene + ozone at $\beta = 0.15$. (a) the 1N layer, where the mass of products are highest in the moderately oxidized and semi-volatile ranges. (b) the 0N layer, where the mass is highly oxidized and lower in volatility.

treat the formation and aging of organonitrates under high-NO$_x$ conditions, and released a complete implementation of this code in MATLAB.

There are relatively few experimental constraints on the behavior of organonitrates in SOA, especially for multi-generational aging. Unknowns include differences between homogeneous and heterogeneous oxidation and the fate of nitrates after fragmentation. As a simplification we have assumed that homogeneous and heterogeneous product distributions are the same, and that fragmentation breaks the weakest bond in the organonitrate, assumed to be the O–NO$_2$ bond. However, it is certain that semi-volatile products (nitrates and non-nitrates alike) will react relatively rapidly in the gas phase and consequently that any first-generation semi-volatile products will not be long lived in the atmosphere.

We explored the aging chemistry of SOA under conditions typical of chamber experiments. During multi-generational aging under high-NO$_x$ conditions, the contribution of organonitrates to organic mass is similar to non-nitrate organics. This contribution of organonitrates to aerosol mass can be large even though the actual nitrate (–ONO$_2$) mass is low, because the N:C of condensed-phase organonitrates can be low. We also reproduced the enhancement of aerosol production in the presence of NO$_x$, under conditions such as high mass loadings or low volatility precursors. This showed that the VBS is capable of accounting for these effects on ex-
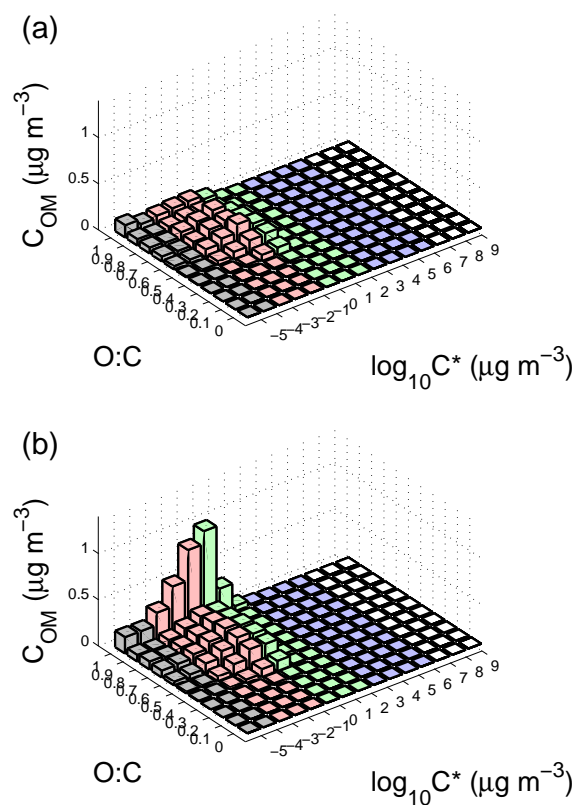
tensive organic chemistry and emphasized the important role that NO$_x$ plays as part of the aging process.

References

Aiken, A. C., De Foy, B., Wiedinmyer, C., Decarlo, P. F., Ulbrich, I. M., Wehrli, M. N., Szidat, S., Prévôt, A. S. H., Noda, J., Wacker, L., Volkamer, R., Fortner, E., Wang, J., Laskin, A., Shutthanandan, V., Zheng, J., Zhang, R., Paredes-Miranda, G., Arnott, W. P., Molina, L. T., Sosa, G., Querol, X., and Jimenez, J. L.: Mexico city aerosol analysis during MILAGRO using high resolution aerosol mass spectrometry at the urban supersite (T0)-Part 2: Analysis of the biomass burning contribution and the

non-fossil carbon fraction, Atmos. Chem. Phys., 10, 5315–5341, 2010.

Andreae, M. O. and Crutzen, P. J.: Atmospheric Aerosols: Biogeochemical Sources and Role in Atmospheric Chemistry, Science (80-.)., 276, 1052–1058, 1997.

Arey, J., Aschmann, S. M., Kwok, E. S. C., and Atkinson, R.: Alkyl Nitrate , Hydroxyalkyl Nitrate , and Hydroxycarbonyl Formation from the NOx - Air Photooxidations of C5 - C8 n-Alkanes, J. Phys. Chem. A., 105, 1020–1027, 2001.

Atherton, C. S.: Organic nitrates in remote marine environments: Evidence for long-range transport, Geophys. Res. Lett., 16, 1289–1292, 1989.

Atkinson, R. and Arey, J.: Atmospheric degradation of volatile organic compounds., Chem. Rev., 103, 4605–38, 2003.

Atkinson, R., Baulch, D. L., Cox, R. A., Hampson, R. F., Kerr, J. A., Rossi, M. J., and Troe, J.: Evaluated Kinetic, Photochemical and Heterogeneous Data for Atmospheric Chemistry: Supplement V. IUPAC Subcommittee on Gas Kinetic Data Evaluation for Atmospheric Chemistry, J. Phys. Chem. Ref. Data, 26, 521 – 1011, 1997.

Aumont, B., Szopa, S., and Madronich, S.: Modelling the evolution of organic carbon during its gas-phase tropospheric oxidation: development of an explicit model based on a self generating approach, Atmos. Chem. Phys., 5, 2497–2517, 2005.

Bond, T. C., Streets, D. G., Yarber, K. F., Nelson, S. M., Woo, J.-H., and Klimont, Z.: A technology-based global inventory of black and organic carbon emissions from combustion, J. Geophys. Res., 109, 1–43, 2004.

Chacon-Madrid, H. J., Presto, A. A., and Donahue, N. M.: Functionalization vs. fragmentation: n-aldehyde oxidation mechanisms and secondary organic aerosol formation., Phys. Chem. Chem. Phys., 12, 13 975–13 982, 2010.

Chen, X., Hopke, P. K., and Carter, W. P. L.: Secondary organic aerosol from ozonolysis of biogenic volatile organic compounds: chamber studies of particle and reactive oxygen species formation, Environ. Sci. Technol., 45, 276–282, 2011.

Chhabra, P. S., Flagan, R. C., and Seinfeld, J. H.: Elemental analysis of chamber organic aerosol using an aerodyne high-resolution aerosol mass spectrometer, Atmos. Chem. Phys., 10, 4111–4131, 2010.

Cronn, D. R., Charlson, R. J., Knights, R. L., Crittenden, A. L., and Appel, B. R.: A Survey Of The Molecular Nature Of Primary And Secondary Components Of Particles In Urban Air By High-Resolution Mass Spectrometry, Atmos. Environ., 10, 929–937, 1977.

Crowley, J. N., Thieser, J., Tang, M. J., Schuster, G., Bozem, H., Beygi, Z. H., Fischer, H., Diesch, J. M., Drewnick, F., Borrmann, S., Song, W., Yassaa, N., Williams, J., Pöhler, D., Platt, U., and Lelieveld, J.: Variable lifetimes and loss mechanisms for NO 3 and N 2O 5 during the DOMINO campaign: Contrasts between marine, urban and continental air, Atmos. Chem. Phys., 11, 10 853–10 870, 2011.

Day, D. A., Liu, S., Russell, L. M., and Ziemann, P. J.: Organonitrate group concentrations in submicron particles with high nitrate and organic fractions in coastal southern California, Atmos. Environ., 44, 1970–1979, 2010.

de Gouw, J. and Jimenez, J. L.: Organic aerosols in the Earth's atmosphere., Environ. Sci. Technol., 43, 7614–7618, 2009.

Dockery, D. W., Pope, C. A., Xu, X., Spengler, J. D., Ware, J. H., Fay, M. E., Ferris, B. G., and Speizer, F. E.: An Association Between Air Pollution and Mortality in Six Cities, N. Engl. J. Med., 329, 1753–1759, 1993.

Donahue, N. M.: A two-dimensional volatility basis set - Part 2: Diagnostics of organic-aerosol evolution, Atmos. Chem. Phys., 12, 615–634, 2012.

Donahue, N. M., Robinson, A. L., Stanier, C. O., and Pandis, S. N.: Coupled partitioning, dilution, and chemical aging of semivolatile organics., Environ. Sci. Technol., 40, 2635–43, 2006.

Donahue, N. M., Epstein, S. A., Pandis, S. N., and Robinson, A. L.: A two-dimensional volatility basis set: 1. organic-aerosol mixing thermodynamics, Atmos. Chem. Phys., 11, 3303–3318, 2011.

Donahue, N. M., Henry, K. M., Mentel, T. F., Kiendler-Scharr, A., Spindler, C., Bohn, B., Brauers, T., Dorn, H. P., Fuchs, H., Tillmann, R., Wahner, A., Saathoff, H., Naumann, K.-H., Möhler, O., Leisner, T., Müller, L., Reinnig, M.-C., Hoffmann, T., Salo, K., Hallquist, M., Frosch, M., Bilde, M., Tritscher, T., Barmet, P., Praplan, A. P., DeCarlo, P. F., Dommen, J., Prévôt, A. S. H., and Baltensperger, U.: Aging of biogenic secondary organic aerosol via gas-phase OH radical reactions, Proc. Natl. Acad. Sci. U. S. A., 109, 13 503–8, 2012.

Donahue, N. M., Chuang, W., Epstein, S. A., Kroll, J. H., Worsnop, D. R., Robinson, A. L., Adams, P. J., and Pandis, S. N.: Why do organic aerosols exist? Understanding aerosol lifetimes using the two-dimensional volatility basis set, Environ. Chem., 10, 151, 2013.

Donahue, N. M., Robinson, A. L., Trump, E. R., Riipinen, I., and Kroll, J. H.: Volatility and Aging of Atmospheric Organic Aerosol, Top. Curr. Chem., 2014.

Elrod, M. J.: Kinetics study of the aromatic bicyclic peroxy radical + NO reaction: overall rate constant and nitrate product yield measurements., J. Phys. Chem. A., 115, 8125–30, 2011.

Farmer, D. K., Matsunaga, A., Docherty, K. S., Surratt, J. D., Seinfeld, J. H., Ziemann, P. J., and Jimenez, J. L.: Response of an aerosol mass spectrometer to organonitrates and organosulfates and implications for atmospheric chemistry, Proc. Natl. Acad. Sci. U. S. A., 107, 6670–6675, 2010.

Fry, J. L., Draper, D. C., Zarzana, K. J., Campuzano-Jost, P., Day, D. a., Jimenez, J. L., Brown, S. S., Cohen, R. C., Kaser, L., Hansel, A., Cappellin, L., Karl, T., Hodzic Roux, A., Turnipseed, A., Cantrell, C., Lefer, B. L., and Grossberg, N.: Observations of gas- and aerosol-phase organic nitrates at BEACHON-RoMBAS 2011, Atmos. Chem. Phys., 13, 8585–8605, 2013.

Garnes, L. A. and Allen, D. T.: Size Distributions of Organonitrates in Ambient Aerosol Collected in Houston, Texas, Aerosol Sci. Technol., 36, 983–992, 2002.

Goldstein, A. H. and Galbally, I. E.: Known and Unexplored Organic Constituents in the Earth's Atmosphere, Environ. Sci. Technol., 41, 1514–1521, 2007.

Hallquist, M., Wenger, J. C., Baltensperger, U., Rudich, Y., Simpson, D., Claeys, M., and Dommen, J.: The formation, properties and impact of secondary organic aerosol: current and emerging issues, Atmos. Chem. Phys., 9, 5155–5236, 2009.

He, Q.-f., Ding, X., Wang, X.-m., Yu, J.-z., Fu, X.-x., and Liu, T.-y.: Organosulfates from Pinene and Isoprene over the Pearl River Delta, South China: Seasonal Variation and Implication in Formation Mechanisms, Environ. Sci. Technol., 2014.

Henry, K. M. and Donahue, N. M.: Photochemical aging of α-pinene secondary organic aerosol: effects of OH radical sources and photolysis., J. Phys. Chem. A, 116, 5932–5940, 2012.

Jimenez, J. L., Canagaratna, M. R., Donahue, N. M., Prévôt, A. S. H., Zhang, Q., Kroll, J. H., DeCarlo, P. F., Allan, J. D., Coe, H., Ng, N. L., Aiken, A. C., Docherty, K. S., Ulbrich, I. M., Grieshop, A. P., Robinson, A. L., Duplissy, J., Smith, J. D., Wilson, K. R., Lanz, V. A., Hueglin, C., Sun, Y. L., Tian, J., Laaksonen, A., Raatikainen, T., Rautiainen, J., Vaattovaara, P., Ehn, M., Kulmala, M., Tomlinson, J. M., Collins, D. R., Cubison, M. J., Dunlea, E. J., Huffman, J. A., Onasch, T. B., Alfarra, M. R., Williams, P. I., Bower, K., Kondo, Y., Schneider, J., Drewnick, F., Borrmann, S., Weimer, S., Demerjian, K., Salcedo, D., Cottrell, L., Griffin, R., Takami, A., Miyoshi, T., Hatakeyama, S., Shimono, A., Sun, J. Y., Zhang, Y. M., Dzepina, K., Kimmel, J. R., Sueper, D., Jayne, J. T., Herndon, S. C., Trimborn, A. M., Williams, L. R., Wood, E. C., Middlebrook, A. M., Kolb, C. E., Baltensperger, U., and Worsnop, D. R.: Evolution of organic aerosols in the atmosphere., Science (80-.)., 326, 1525–1529, 2009.

Kalberer, M., Paulsen, D., Sax, M., Steinbacher, M., Dommen, J., Prévôt, A. S. H., Fisseha, R., Weingartner, E., Frankevich, V., Zenobi, R., and Baltensperger, U.: Identification of Polymers as Major Components of Atmospheric Organic Aerosols, Science (80-.)., 303, 1659–1662, 2004.

Kanakidou, M., Seinfeld, J. H., Pandis, S. N., Barnes, I., Dentener, F. J., Facchini, M. C., Van Dingenen, R., Ervens, B., Nenes, A., Nielsen, C. J., Swietlicki, E., Putaud, J. P., Balkanski, Y., Fuzzi, S., Horth, J., Moortgat, G. K., Winterhalter, R., Myhre, C. E. L., Tsigaridis, K., Vignati, E., Stephanou, E. G., and Wilson, J. C.: Organic aerosol and global climate modelling: a review, Atmos. Chem. Phys., 5, 1053–1123, 2005.

Kroll, J. H., Ng, N. L., Murphy, S. M., Flagan, R. C., and Seinfeld, J. H.: Secondary organic aerosol formation from isoprene photooxidation., Environ. Sci. Technol., 40, 1869–1877, 2006.

Kroll, J. H., Smith, J. D., Che, D. L., Kessler, S. H., Worsnop, D. R., and Wilson, K. R.: Physical chemistry of aerosols., Phys. Chem. Chem. Phys., 11, 8007–8014, 2009.

Kroll, J. H., Donahue, N. M., Jimenez, J. L., Kessler, S. H., Canagaratna, M. R., Wilson, K. R., Altieri, K. E., Mazzoleni, L. R., Wozniak, A. S., Bluhm, H., Mysak, E. R., Smith, J. D., Kolb, C. E., and Worsnop, D. R.: Carbon oxidation state as a metric for describing the chemistry of atmospheric organic aerosol., Nat. Chem., 3, 133–139, 2011.

Kwok, E. S. C. and Atkinson, R.: Estimation Of Hydroxyl Radical Reaction Rate Constants For Gas-Phase Organic Compounds Using A Structure-Reactivity Relationship: An Update, Atmos. Environ., 29, 1685–1695, 1995.

Lane, T. E., Donahue, N. M., and Pandis, S. N.: Simulating secondary organic aerosol formation using the volatility basis-set approach in a chemical transport model, Atmos. Environ., 42, 7439–7451, 2008a.

Lane, T. E., Donahue, N. M., and Pandis, S. N.: Effect of NOx on Secondary Organic Aerosol Concentrations, Environ. Sci. Technol., 42, 6022–6027, 2008b.

Lim, Y. B. and Ziemann, P. J.: Effects of molecular structure on aerosol yields from OH radical-initiated reactions of linear, branched, and cyclic alkanes in the presence of NOx., Environ. Sci. Technol., 43, 2328–34, 2009.

Liu, S., Shilling, J. E., Song, C., Hiranuma, N., Zaveri, R. A., and Russell, L. M.: Hydrolysis of Organonitrate Functional Groups in Aerosol Particles, Aerosol Sci. Technol., 46, 1359–1369, 2012.

Logan, J. A., Prather, M. J., Wofsy, S. C., and McElroy, M. B.: Tropospheric chemistry: A global perspective, J. Geophys. Res., 86, 7210–7254, 1981.

Minguillón, M. C., Perron, N., Querol, X., Szidat, S., Fahrni, S. M., Alastuey, A., Jimenez, J. L., Mohr, C., Ortega, A. M., Day, D. A., Lanz, V. A., Wacker, L., Reche, C., Cusack, M., Amato, F., Kiss, G., Hoffer, A., Decesari, S., Moretti, F., Hillamo, R., Teinilä, K., Seco, R., Pemñuelas, J., Metzger, A., Schallhart, S., Müller, M., Hansel, A., Burkhart, J. F., Baltensperger, U., and Prévôt, A. S. H.: Fossil versus contemporary sources of fine elemental and organic carbonaceous particulate matter during the DAURE campaign in Northeast Spain, Atmos. Chem. Phys., 11, 12 067–12 084, 2011.

Murphy, B. N., Donahue, N. M., Fountoukis, C., Dall'Osto, M., O'Dowd, C., Kiendler-Scharr, A., and Pandis, S. N.: Functionalization and fragmentation during ambient organic aerosol aging: application of the 2-D volatility basis set to field studies, Atmos. Chem. Phys., 12, 10 797–10 816, 2012.

Murphy, B. N., Donahue, N. M., Robinson, A. L., and Pandis, S. N.: A naming convention for atmospheric organic aerosol, Atmos. Chem. Phys., 14, 5825–5839, 2014.

Mylonas, D. T., Allen, D. T., Ehrman, S. H., and Pratsinis, S. E.: The Sources And Size Distributions Of Organonitrates In Los Angeles Aerosol, Atmos. Environ., 25A, 2855–2861, 1991.

Ng, N. L., Chhabra, P. S., Chan, A. W. H., Surratt, J. D., Kroll, J. H., Kwan, A. J., McCabe, D. C., Wennberg, P. O., Sorooshian, A., Murphy, S. M., Dalleska, N. F., Flagan, R. C., and Seinfeld, J. H.: Effect of NOx level on secondary organic aerosol (SOA) formation from the photooxidation of terpenes, Atmos. Chem. Phys., 7, 5159–5174, 2007.

Odum, J. R., Hoffmann, T., Bowman, F., Collins, D., Flagan, R. C., and Seinfeld, J. H.: Gas/Particle Partitioning and Secondary Organic Aerosol Yields, Environ. Sci. Technol., 30, 2580–2585, 1996.

Pandis, S. N., Paulson, S. E., Seinfeld, J. H., and Flagan, R. C.: Aerosol Formation in the Photooxidation of Isoprene and β-Pinene, Atmos. Environ., 25, 997–1008, 1991.

Pankow, J. F.: An Absorption Model Of The Gas / Aerosol Partitioning Involved In The Formation Of Secondary Organic Aerosol, Atmos. Environ., 28, 189–193, 1994.

Pankow, J. F. and Asher, W. E.: SIMPOL.1: a simple group contribution method for predicting vapor pressures and enthalpies of vaporization of multifunctional organic compounds, Atmos. Chem. Phys., 8, 2773–2796, 2008.

Pathak, R. K., Presto, A. A., Lane, T. E., Stanier, C. O., Donahue, N. M., and Pandis, S. N.: Ozonolysis of α-pinene: parameterization of secondary organic aerosol mass fraction, Atmos. Chem. Phys., 7, 3811–3821, 2007.

Peng, R. D., Dominici, F., Pastor-Barriuso, R., Zeger, S. L., and Samet, J. M.: Seasonal analyses of air pollution and mortality in 100 US cities, Am. J. Epidemiol., 161, 585–594, 2005.

Pope, C. A., Ezzati, M., and Dockery, D. W.: Fine-Particulate Air Pollution and Life Expectancy in the United States, N. Engl. J. Med., 360, 376–386, 2009.

Presto, A. A. and Donahue, N. M.: Investigation of alpha-pinene + ozone secondary organic aerosol formation at low total aerosol

mass., Environ. Sci. Technol., 40, 3536–3543, 2006.

Presto, A. A., Hartz, K. E. H., and Donahue, N. M.: Secondary organic aerosol production from terpene ozonolysis. 2. Effect of NOx concentration., Environ. Sci. Technol., 39, 7046–54, 2005.

Rollins, A. W., Kiendler-Scharr, A., Fry, J., Brauers, T., Brown, S. S., Dorn, H.-P., Dubé, W. P., Fuchs, H., Mensah, A., Mentel, T. F., Rohrer, F., Tillmann, R., Wegener, R., Wooldridge, P. J., and Cohen, R. C.: Isoprene oxidation by nitrate radical: alkyl nitrate and secondary organic aerosol yields, Atmos. Chem. Phys., 9, 6685–6703, 2009.

Rollins, A. W., Fry, J. L., Hunter, J. F., Kroll, J. H., Worsnop, D. R., Singaram, S. W., and Cohen, R. C.: Elemental analysis of aerosol organic nitrates with electron ionization high-resolution mass spectrometry, Atmos. Meas. Tech., 3, 301–310, 2010.

Russell, A. R., Valin, L. C., and Cohen, R. C.: Trends in OMI NO2 observations over the US: effects of emission control technology and the economic recession, Atmos. Chem. Phys. Discuss., 12, 12 197–12 209, 2012.

Russell, L. M., Bahadur, R., and Ziemann, P. J.: Identifying organic aerosol sources by comparing functional group composition in chamber and atmospheric particles., Proc. Natl. Acad. Sci. U. S. A., 108, 3516–21, 2011.

Seinfeld, J. H. and Pandis, S. N.: Atmospheric Chemistry and Physics: From Air Pollution to Climate Change, Second Edition, John Wiley & Sons, Inc., 2006.

Shilling, J. E., Chen, Q., King, S. M., Rosenoern, T., Kroll, J. H., Worsnop, D. R., DeCarlo, P. F., and Aiken, A. C.: Loading-dependent elemental composition of α-pinene SOA particles, Atmos. Chem. Phys., 9, 771–782, 2009.

Shilling, J. E., Zaveri, R. A., Fast, J. D., Kleinman, L., Alexander, M. L., Canagaratna, M. R., Fortner, E., Hubbe, J. M., Jayne, J. T., Sedlacek, A., Setyan, A., Springston, S., Worsnop, D. R., and Zhang, Q.: Enhanced SOA formation from mixed anthropogenic and biogenic emissions during the CARES campaign, Atmos. Chem. Phys., 13, 2091–2113, 2013.

Shrivastava, M. K., Lane, T. E., Donahue, N. M., Pandis, S. N., and Robinson, A. L.: Effects of gas particle partitioning and aging of primary emissions on urban and regional organic aerosol concentrations, J. Geophys. Res., 113, D18 301, 2008.

Spracklen, D. V., Jimenez, J. L., Carslaw, K. S., Worsnop, D. R., Evans, M. J., Mann, G. W., Zhang, Q., Canagaratna, M. R., Allan, J., Coe, H., McFiggans, G., Rap, A., and Forster, P.: Aerosol mass spectrometer constraint on the global secondary organic aerosol budget, Atmos. Chem. Phys., 11, 12 109–12 136, 2011.

Thompson, A. M. and Cicerone, R. J.: Clouds and Wet Removal as Causes of Variability in the Trace-Gas Composition of the Marine Troposphere, J. Geophys. Res., 87, 8811–8826, 1982.

Trump, E. R. and Donahue, N. M.: Oligomer formation within secondary organic aerosols: equilibrium and dynamic considerations, Atmos. Chem. Phys., 14, 3691–3701, 2014.

Trump, E. R., Riipinen, I., and Donahue, N. M.: Interactions between atmospheric ultrafine particles and secondary organic aerosol mass : a model study, Boreal Environ. Res., 19, 352–362, 2014.

Turpin, B. J. and Huntzicker, J. J.: Identification Of Secondary Organic Aerosol Episodes And Quantitation Of Primary And Secondary Organic Aerosol Concentrations During SCAQS, Atmos. Environ., 29, 3527–3544, 1995.

Turpin, B. J., Saxena, P., and Andrews, E.: Measuring and simulating particulate organics in the atmosphere: problems and prospects, Atmos. Environ., 34, 2983–3013, 2000.

Weber, R. J., Sullivan, A. P., Peltier, R. E., Russell, A., Yan, B., Zheng, M., de Gouw, J., Warneke, C., Brock, C., Holloway, J. S., Atlas, E. L., and Edgerton, E.: A study of secondary organic aerosol formation in the anthropogenic-influenced southeastern United States, J. Geophys. Res., 112, 1–13, 2007.

Wittig, A. E., Anderson, N., Khlystov, A. Y., Pandis, S. N., Davidson, C. I., and Robinson, A. L.: Pittsburgh air quality study overview, Atmos. Environ., 38, 3107–3125, 2004.

Yeh, G. K. and Ziemann, P. J.: Alkyl Nitrate Formation from the Reactions of C8 - C14 n-Alkanes with OH Radicals in the Presence of NO: Measured Yields with Essential Corrections for Gas-Wall Partitioning, J. Phys. Chem. A., 118, 8797–8806, 2014.

Zhang, J., Dransfield, T., and Donahue, N. M.: On the Mechanism for Nitrate Formation via the Peroxy Radical + NO Reaction, J. Phys. Chem. A, 108, 9082–9095, 2004.

Zhang, J., Huff Hartz, K. E., Pandis, S. N., and Donahue, N. M.: Secondary organic aerosol formation from limonene ozonolysis: homogeneous and heterogeneous influences as a function of NOx., J. Phys. Chem. A., 110, 11 053–11 063, 2006.

Zhang, Q., Jimenez, J. L., Canagaratna, M. R., Allan, J. D., Coe, H., Ulbrich, I., Alfarra, M. R., Takami, A., Middlebrook, a. M., Sun, Y. L., Dzepina, K., Dunlea, E., Docherty, K., DeCarlo, P. F., Salcedo, D., Onasch, T., Jayne, J. T., Miyoshi, T., Shimono, A., Hatakeyama, S., Takegawa, N., Kondo, Y., Schneider, J., Drewnick, F., Borrmann, S., Weimer, S., Demerjian, K., Williams, P., Bower, K., Bahreini, R., Cottrell, L., Griffin, R. J., Rautiainen, J., Sun, J. Y., Zhang, Y. M., and Worsnop, D. R.: Ubiquity and dominance of oxygenated species in organic aerosols in anthropogenically-influenced Northern Hemisphere midlatitudes, Geophys. Res. Lett., 34, L13 801, 2007.

Zhang, Y. L., Perron, N., Ciobanu, V. G., Zotter, P., Minguilón, M. C., Wacker, L., Prévôt, A. S. H., Baltensperger, U., and Szidat, S.: On the isolation of OC and EC and the optimal strategy of radiocarbon-based source apportionment of carbonaceous aerosols, Atmos. Chem. Phys., 12, 10 841–10 856, 2012.

Ziemann, P. J. and Atkinson, R.: Kinetics, products, and mechanisms of secondary organic aerosol formation., Chem. Soc. Rev., 41, 6582–605, 2012.